Novel Second-Order Transfer Section for Frequency-Selective Response Generation in Comb Filters

Roman Sotner, *Member, IEEE*, Dmitrii Semenov, Darius Andriukaitis, *Member, IEEE*, Marek Svoboda, and Ladislav Polak, *Member, IEEE*

***Abstract*— This article introduces a novel unified second-order filtering topology for standard band-reject (sBR) and inverting band-reject filter, enabling selective response generation. It is applied in the design of special comb filters that allow attenuation as well as amplification of specific bands. The presented solution offers several advantageous features in topology, enhanced cascadability, better parameter-setting performance, and the use of readily available off-the-shelf components, all while reducing overall costs. This is a significant improvement compared to the previous solutions in this field, which relied on a very expensive CMOS process. The topology employs a combination of an operational transconductance amplifier (OTA) and a current feedback amplifier. The intended center frequencies and transfer values of the comb filter are set to 50 Hz (−20 dB), 1 kHz (+26 dB), 10 kHz (+17 dB), and 100 kHz (−30 dB). The comb filter was experimentally verified via simulations as well as laboratory measurements utilizing LT1228 devices in a fabricated prototype.**

***Index Terms*— Band-reject filter, comb filter, current feedback amplifier, inverse filter, notch, operational transconductance amplifier (OTA).**

I. Introduction

HIGHLY selective frequency filtering constitutes a significant component of all analog signal processing systems [1]. Effectively optimizing the frequency response of signals distributed from multiple sensors and sensing paths is crucial for many systems. It necessitates the equalization and compensation of frequency response imbalances (losses/gains) and selective distortions. These particular features are advantageous for modern sensing readout and adaptive signal processing [2].

Received 24 September 2024; revised 3 February 2025; accepted 14 February 2025. Date of publication 7 March 2025; date of current version 27 March 2025. This work was supported by the Internal Grant of Brno University of Technology (BUT) under Project FEKT-S-23-8191. This project has received funding from the Research Council of Lithuania (LMTLT), Agreement No. S-AUEI-23-1 (22-12-2023). This work was supported by the Institutional Support of the Ministry of Defence of the Czech Republic. The Associate Editor coordinating the review process was Dr. Tarikul Islam. *(Corresponding author: Roman Sotner.)*

Roman Sotner is with the Faculty of Electrical Engineering and Communication, Brno University of Technology, 616 00 Brno, Czech Republic, and also with the Department of Electrical Engineering, Faculty of Military Technology, University of Defence Brno, 602 00 Brno, Czech Republic (e-mail: sotner@vut.cz; roman.sotner@unob.cz).

Dmitrii Semenov, Marek Svoboda, and Ladislav Polak are with the Faculty of Electrical Engineering and Communication, Brno University of Technology, 616 00 Brno, Czech Republic (e-mail: 240689@vut.cz; 211319@vut.cz; polakl@vut.cz).

Darius Andriukaitis is with the Department of Electronics Engineering, Faculty of Electrical and Electronics Engineering, Kaunas University of Technology, 51368 Kaunas, Lithuania (e-mail: darius.andriukaitis@ktu.lt).

Digital Object Identifier 10.1109/TIM.2025.3548818

A. Comb Filters

Typical solutions for suppressing selective frequency distortions include so-called comb filters [3], [4], [5], [6], [7], [8], [9]. These filters are essentially represented by a bank of filters and the sum/difference of their responses (such as bandpass [3], all-pass [7], and inverting bandpass responses [5], [6]) with the input signal or a cascade of band-reject/notch filters [4], [8], [9]. Analyzing known comb-filter solutions [3], [4], [5], [6], [7], [8], [9], all of which consist of four sections (as summarized in Table I), several key findings emerge: 1) the frequency responses of known solutions primarily offer attenuation at specific selective frequencies (bands); 2) impedance separation (high input or low-output frequency independent impedance) of sections is unavailable [4], [5], [6], [7], [8], [9], and an appropriate (low or high) final output/input impedance of the comb filter is not ensured [8], [9]; 3) sections used for comb response generation serve a single purpose in all cases; 4) some sections are quite complex [5], [6], [7], contributing to the overall complexity of the comb filter; and 5) attention in design is typically focused on Hertz and hundreds of Hertz bands due to exclusive electrocardiogram applications (for suppressing electrical power network distortion in medical instrumentation). Based on an overview of previously reported solutions and to the best of the author's knowledge, the standard band-reject (sBR) filter and the inverse response of the band-reject filter (iBR) have not been used for the construction of comb filters [3], [4], [5], [6], [7], [8], [9] or are these responses available in a single section simultaneously. Our solution, presented in this article, enables selective subband filtering based not only on attenuation but also on amplification at targeted frequencies. Therefore, our work addresses the gap in the design of comb filters for more sophisticated and wideband applications in modern sensing and signal distribution systems.

B. Inverse Response Filters

Recent years have seen increased attention toward inverse response analog filters due to their nonstandard transfer responses compared to standard transfer functions [1]. Apart from their relevance in standard filtering responses [1], the significance of inverse response filters becomes evident in the synthesis of comb filters. Research in this domain has produced numerous intriguing solutions (e.g., [10], [11], [12], [13], [14], [15], [16], [17], [18], [19], [20]). However, many

TABLE I
COMPARISON OF FOUR SECTION-BASED COMB FILTERS

Solution	Type of section transfer response	Number of active/passive (floating) elements in section; number of packages	Operation without summation/ difference of multiple responses	Attenuations setting at selected frequency available in response	Gain setting at selected frequency available in response	Tested operational frequency range (purpose)	Impedance separation of each section (low output or high input impedance)	Overall impedance separation of output (load allowed)	Implementation	Verification	Figure of Merit (FOM)
[3]	BP	1/4(4);1	No	Yes	No	1 Hz→500 Hz (ECG)	Yes	Yes	Discrete (opamps LM741)	Simulation	0.20
[4]	sBR	2/2(1);-	Yes	Yes	No	0 Hz→600 Hz (ECG)	No	Yes	CMOS (OTAs, 0.5 μm)	Simulation	0.25
[5]	IBP	3/5(0);-	No	Yes	No	0 Hz→500 Hz (ECG)	No	Yes	CMOS (CCII, 0.18 μm)	Simulation	0.13
[6]	IBP	3/5(0);3	No	Yes	No	0 Hz→500 Hz (ECG)	No	Yes	Discrete (AD844)	Both	0.13
[7]	AP	3/4(4);>3	No	Yes	No	0 Hz→500 Hz (ECG)	No	Yes	Discrete (AD844)	Both	0.14
[8]	sBR	1/3(1);-	Yes	Yes	No	0 Hz→450 Hz (ECG)	No	No	CMOS (VDTA, 0.18 μm)	Simulations	0.25
[9]	sBR	1/4(1);2	Yes	Yes	No	0 Hz→450 Hz (ECG)	No	No	Discrete (MAX435, AD844)	Simulation	0.20
Fig. 2	sBR,iBR	3/3(3);2	Yes	Yes	Yes	10 Hz→1 MHz (*)	Yes	Yes	Discrete (LT1228)	Both	0.33

BP – band-pass, IBP – inverting band-pass, AP – all pass, sBR – standard band-reject/notch, iBR – inverse band-reject, OTA – operational transconductance amplifier, CCII – current conveyor of second generation, VDTA – voltage differencing transconductance amplifier, ECG – electrocardiogram, *general purpose from sub Hz, audio and long wave sensing and processing.
Figure of Merit (FOM) = (number of transfer responses created by a single section) / (number of active elements + passive elements in single section); further parameters such as power consumption and noise, cannot be easily compared due to the lack of available data and the antipodal differences between discrete and integrated solutions (lacks of parameters being more common with discrete solutions).

of these solutions exhibit a considerable degree of redundancy for applications in comb filters, owing to their universal nature. A comprehensive review of inverse response filters is available in [21]. Nonetheless, many of these structures, being universal, employ complex topologies (with a high number of passive elements) and lack electronically adjustable features. Consequently, their suitability for comb filters is questionable. Table II illustrates typical solutions of inverse response filters. Some of these solutions are highly versatile, offering three or more transfer responses [10], [11], [12], [13], [14], [16], [17], [18], [19], [20]. However, this versatility comes at the cost of topologically complex solutions that utilize a high number of active [12], [13] or passive [10], [11], [15], [16], [17], [18], [20] elements. Discrete solutions entail a relatively large number of IC packages [10], [11], [16], [18].

Many of the published works are redundant [10], [11], [12], [13], [14], [16], [17], [18], [19], [20] or even unsuitable [15] for the cascade synthesis of comb filters. In fact, only the inverse response (iBR) available in [10], [12], [13], [16], [17], and [19] is applicable in comb filters. Some degree of electronic adjustability or setting is allowed in a limited number of solutions [12], [13] (focused on the quality factor of iBR), [17] (focused on iBR center frequency tuning by several sets of parameters). While a limited number of existing electronically tunable inverse response filters enable electronic tunability of cutoff frequencies [22], [23] and quality factor [22], these solutions typically utilize four operational transconductance amplifiers (OTAs) [22] or voltage differencing transconductance amplifiers (VDTAs) [23] (which include three OTAs in the principle of a single VDTA). First-order inverse filters have become increasingly attractive in recent years due to their significance in controller design [24], [25]. However, these solutions typically have a low quality factor and are unable to generate the highly selective transfer responses required for comb-filter design (such as sBR and iBR). To the best of the author's knowledge, a specific solution allowing the simultaneous design of second-order sBR and iBR has not been available in recently reported solutions in a compact topology. Based on figures of merits (Tables I and II), the proposed solution reaches significant qualitative and quantitative performance in comparison to known solutions in the field of the most important comb and second-order inverse filters for purposes described in this work.

C. Recent Advances in Special Response Filters

Nako and Psychalinos [26] and Nako et al. [27] presented highly useful solutions known as formant filters, which are applied in processing voice vowels. However, unlike the filter presented in this article, these solutions focus on active resonators based on specialized low-pass sections, rather than combining inverse and standard response filters in the same cascade. These formant filters create resonator responses (selective passband amplification) and anti-resonator responses (selective stopband attenuation) [26], [27]. The topologies are based on multiloop feedback structures, they utilize numerous components, including lossy/lossless integrators built with simple OTAs, as recommended in [28]. While this approach allows for straightforward electronic configurability, it increases the overall complexity when compared to our solution. Additionally, the cascading principle is not employed in [27]. Instead, the filters rely on the sum of several parallel paths, without combining selective amplification (standard and inverse response) or attenuation in resulting response. As a result, the solutions presented in [26] and [27] are excluded from the comparison Table I and discussed separately in this section.

TABLE II
COMPARISON OF IMPORTANT FEATURES AND TYPICAL SECOND-ORDER INVERSE RESPONSE FILTERS

Work	Number of active/passive (floating) elements	Number of IC packages	Type of generated responses	Redundant response for cascade implementation in comb filter	Impedance separation of each section (low output or high input impedance) for cascading (voltage mode)	Suitability for comb filters	Tested operational frequency band	Active device used	Implementation	Verification	Figure of Merit (FOM)
[10]	3/6(0,3,4)	3	iLP, iBP, iHP, iBR	3	Yes	Yes	1 kHz→100 kHz	CFOA	Discrete (AD844)	Both	8.3
[11]	3/5 (0)	3	iLP, iBP, iHP	3	Yes	No	10 Hz→100 kHz	CFOA	Discrete (AD844)	Simulations	$9.1{\cdot}10^{2}$
[12]	4-5/2 (0)	-	iLP, iBP, iHP, iBR	3	Yes	Yes	10 kHz→1 GHz	OTA	CMOS (0.18 μm)	Simulations	$1.0{\cdot}10^{4}$
[13]	2-4/2 (0)	-	iLP, iBP, iHP, iBR	3	Yes	Yes	100 kHz→100 MHz	VDTA	CMOS (0.18 μm)	Simulations	$1.1{\cdot}10^{2}$
[14]	2/4 (4)	-	iLP, iBP, iHP	3	Yes	No	10 kHz→50 MHz	CDBA	CMOS (0.35 μm)	Simulations	$5.6{\cdot}10^{2}$
[15]	2/8 (6)	2	iBP	1	Yes	No	10 Hz→1 MHz	CDBA	Discrete (AD844)	Simulations	$9.1{\cdot}10^{3}$
[16]	2/6 (4)	4	iLP, iBP, iHP, iBR, iAP	4	Yes	Yes	100 Hz→10 MHz	CDBA	Discrete (AD844)	Simulations	$8.3{\cdot}10^{3}$
[17]	1/6 (4)	2	iLP, iBP, iHP, iBR	3	Yes	Yes	1 kHz→100 MHz	CDBA	Both (0.35 μm+AD844)	Simulations	$1.0{\cdot}10^{4}$
[18]	2/5 (5)	4	iLP, iBP, iHP	3	Yes	No	1 Hz→10 MHz	OTRA	Both (0.35 μm+AD844)	Both	$1.0{\cdot}10^{6}$
[19]	2/4 (0,1)	-	iLP, iBP, iHP, iBR	3	No	N/A	1 Hz→10 MHz	VCII	CMOS (0.18 μm)	Simulations	$1.1{\cdot}10^{6}$
[20]	2-3/5-8 (3,4)	-	iLP, iBP, iHP	3	No	No	1 Hz→10 MHz	VCII	CMOS (0.18 μm)	Simulations	$7.1{\cdot}10^{5}$
Fig. 2	3/3 (3)	2	sBR, iBR	0	Yes	Yes	10 Hz→1 MHz	OTA+ CFOA	Discrete (LT1228)	Both	$1.7{\cdot}10^{4}$

Our design focuses on band-reject and inverse band-reject transfer response, both available within a single circuit topology through the implementation of the LT1228 device. This represents a different approach to the solutions presented in [26] and [27]. While some sections or inverse response filters listed in Tables I and II could potentially be implemented in similar comb filters (through without the ability to reconfigure between sBR and isBR frequency responses), this was not tested, and no recommendations were given provided by the authors, who did not focus on this aspect. Consequently, the overall solution for such comb filters would likely be extremely complex in most cases.

An approach involving band-reject and inverse band-reject transfer responses was recently used in [29]. The solution presented in this article addresses several shortcomings found in [29], including the frequency-dependent input/output impedance of the section, which requires additional buffering; the need for a special double-output OTA; and gain/attenuation being restricted to capacitor ratios only. The improvements in our solution are as follows: a low output impedance of the section (allowing for simple cascading without requiring additional buffer), gain/attenuation adjustment in the section thorough a dedicated parameter (independent of capacitor ratios), and the use of a simple, available active device without special features.

Modern audio and voice signal processing [26], [27], [28], [30] represents a significant application area for analog filters. Excellent examples of their use can be found in [26] and [27]. Another important application is in equalization or frequency response correction within sensing paths, where various absorptions or frequency-dependent responses can create significant imbalances across the operational bandwidth [30]. This type of behavior is commonly observed in the responses of acoustic and vibration sensors [30].

D. New Features and Design Targets of the Solution

The proposed comb-filter topology in this article achieves several beneficial goals: 1) it offers a simple and compact topology for each section; 2) it provides a unified topology for both types of transfer responses; 3) the section has low output impedance, facilitating straightforward cascading; 4) it operates effectively from tens of Hertz up to hundreds of kilohertz, with a flat response extending up to 1 MHz; 5) features can be easily adjusted using transconductances and resistor values; 6) the capacitance ratio is fixed at 1 and values can be selected from standard fabrication series, simplifying the design process; and 7) the design can be easily reproduced without the need for expensive fabrication in a CMOS process—a discrete solution of an active device (off-

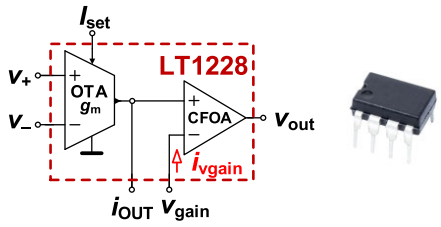

Fig. 1. Internal topology and explanation of LT1228.

the-shelf commercially available type) is used as the core of each section.

This article is organized as follows. Section II presents and elucidates the principle of the proposed sBR/iBR section. Section III provides the specifications of parameters, design targets, and expected features of the four sections forming the comb filter. Experimental results and their accuracy concerning expectations and design targets are discussed in Section IV. Section V presents a straightforward application example of the comb filter for mask shaping and balancing signal tones in duplex communication. Finally, Section VI concludes this work.

II. Band-Reject and Inverting Band-Reject Section

The comb filters utilize band-reject or notch transfer responses to form a complete response. In our case, we employ a circuit topology capable of generating both standard and special inverse band-reject responses of the second order. The proposed circuit is versatile and suitable for both types of transfers. Thus, both filtering responses are accessible without the need to alter the topology.

A. Used Active Device

In this work, we used the commercially available active device LT1228 [31] (see Fig. 1) as the key element of our design. This device integrates a standard OTA [22] and a current feedback operational amplifier (CFOA) [32] within a single DIL8 package. Consequently, both elements combine to form a compact and advanced active subpart suitable for various analog designs. The input differential voltage is transformed through transconductance (g_m) to output current as $i_{\text{OUT}} = (v_+ - v_-) \cdot g_m$ where g_m is adjustable by bias current I_{set}. The CFOA part is defined by ideally infinite transimpedance gain $v_{\text{out}} = Z_{\text{T}} \cdot i_{\text{vgain}}$ (where $Z_{\text{T}} \to \infty$) and by the equality of voltages of both input terminals (+/– of the CFOA part) [31]. The CFOA part serves as voltage amplifier or voltage buffer in many standard cases. However, in our work, we utilize this part in a nonstandard manner as a component of the signal operations in the filter, with the working capacity and feedback aspects addressed by the CFOA.

B. Proposed Filtering Section

The configuration of the section to the intended type of transfer response [sBR(i) or iBR(i)] depends on the input selection of $\text{IC}_{\text{a(i)}}$ (determined by the polarity of $g_{ma(i)}$ based on OTA inputs). The circuit shown in Fig. 2 has a universal symbolical transfer function for both required responses

$$K_{i/\text{sBR}(i)}(s) = \frac{s^2 + \left(\frac{g_{mb(i)}C_{b(i)} \pm g_{ma(i)}C_{a(i)}}{C_{a(i)}C_{b(i)}}\right)s + \frac{g_{mb(i)}}{C_{a(i)}C_{b(i)}R_{(i)}}}{s^2 + \frac{g_{mb(i)}}{C_{a(i)}}s + \frac{g_{mb(i)}}{C_{a(i)}C_{b(i)}R_{(i)}}} \quad (1)$$

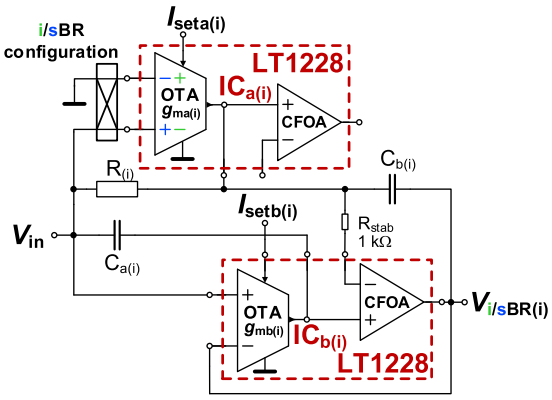

Fig. 2. Proposed second-order topology of standard and inverse band-reject response for design of comb filters.

where the center frequency is determined by

$$f_{C(i)} = \sqrt{\frac{g_{mb(i)}}{C_{a(i)}C_{b(i)}R_{(i)}}} \quad (2)$$

maximal attenuation (minimal gain at f_C) of the sBR

$$\left|K_{\min}\left(f = f_{C(i)}\right)\right| = \frac{g_{mb(i)}C_{b(i)} - g_{ma(i)}C_{a(i)}}{g_{mb(i)}C_{b(i)}} = 1 - \frac{g_{ma(i)}C_{a(i)}}{g_{mb(i)}C_{b(i)}} \quad (3)$$

maximal gain of iBR

$$\left|K_{\max}\left(f = f_{C(i)}\right)\right| = \frac{g_{mb(i)}C_{b(i)} + g_{ma(i)}C_{a(i)}}{g_{mb(i)}C_{b(i)}} = 1 + \frac{g_{ma(i)}C_{a(i)}}{g_{mb(i)}C_{b(i)}} \quad (4)$$

bandwidth of the sBR

$$BW_s = \frac{g_{mb(i)}}{2\pi C_{a(i)}}. \quad (5)$$

The bandwidth of the iBR is given as

$$BW_i = \frac{g_{ma(i)}C_{a(i)} + g_{mb(i)}C_{b(i)}}{2\pi C_{a(i)}C_{b(i)}} \quad (6)$$

which (considering of $C_{a(i)} = C_{b(i)} = C_{(i)}$) is simplified to

$$BW_i = \frac{g_{ma(i)} + g_{mb(i)}}{2\pi C_{(i)}} = \left|K_{\max}\left(f = f_{C(i)}\right)\right| \cdot \frac{g_{mb(i)}}{2\pi C_{(i)}}. \quad (7)$$

Note that both bandwidths are defined by the same way (±3 dB). The −3 dB bandwidth of the pole frequency of iBR is also given as (5), i.e.: $g_{mb(i)}/(2\pi C_{a(i)})$.

C. Most Important Small-Signal Parasitic Effects

Completely surveying all small-signal parasitic elements in detail is challenging. Therefore, the resulting implications of the most important real features are discussed the following text.

The circuit operation of the section is primarily influenced by the grounded parasitic resistance in the node between OTA and CFOA of the $\text{IC}_{\text{b(i)}}$ part (designated as $R_{pb(i)}$). This resistance causes low-frequency attenuation in the passband, as described in the following equation:

$$\left|K_{i/\text{sBR}(i)}(f \to 0)\right| \cong 1 - \frac{1}{g_{mb(i)} \cdot R_{pb(i)}}. \quad (8)$$

A significant impact occurs for $R_{pb(i)} < 100$ kΩ, resulting in an attenuation of around 1–2 dB. Additionally, the stray capacity $C_{pb(i)}$ at the same node affects the gain/attenuation at the center frequency $f_{C(i)}$ as described by

$$\left|K_{\min/\max}\left(f = f_{C(i)}\right)\right| \cong \frac{g_{mb(i)}C_{b(i)}R_{(i)} \pm g_{ma(i)}C_{a(i)}R_{(i)} - C_{pb(i)}}{g_{mb(i)}C_{b(i)}R_{(i)}}. \quad (9)$$

To ensure an insignificant effect on gain/attenuation settings, the ratio $C_{a/b(i)}/C_{pb(i)}$ should be greater than 1000. It is evident that this issue becomes more pronounced at higher frequencies, where the working capacitors $C_{a/b(i)}$ decrease in value (to low hundreds of picofarads and less).

Similar effects such as attenuation or gain variation at the center frequency are caused by the resistance $R_{pa(i)}$ in the node between OTA and CFOA of $IC_{a(i)}$. The gain/attenuation equation is defined similar to the one mentioned above

$$\left|K_{\min/\max}\left(f = f_{C(i)}\right)\right| \cong \frac{g_{mb(i)}C_{b(i)} \pm g_{ma(i)}C_{a(i)}}{g_{mb(i)}C_{b(i)}} + \frac{C_{a(i)}}{g_{mb(i)}R_{pa(i)}C_{b(i)}}. \quad (10)$$

To achieve maximum attenuation, this resistance should be as high as possible, ideally in the range of hundreds of kiloohms. The parasitic capacitance $C_{pa(i)}$ in the node between OTA and CFOA of $IC_{a(i)}$ has a less significant effect when $C_{a/b(i)}/C_{pa(i)} < 10$. However, it can increase the pass-band gain at high frequencies, as described in: $|K_{i/\mathrm{sBR}(i)}(f \to \infty)| \cong 1 + C_{pa(i)}/C_{b(i)}$. This impact is noticeable only when $C_{b(i)}/C_{pa(i)} < 10$. Based on an analysis of ideal simulations, the effect of these factors on the center frequency $f_{C(i)}$ is minimal compared to the previously discussed influences. The impacts of the inequality $C_{a(i)} \neq C_{b(i)}$ are discussed in Section IV.

III. Design of the Comb Filter

When the discussed transfer sections (see Fig. 2) are connected in cascade, the general transfer response of the comb filter has the following form:

$$K_{\mathrm{sum}}(s) = \frac{V_{\mathrm{out}}(s)}{V_{\mathrm{in}}(s)} = \prod_{i=1}^{n} K_{\mathrm{sBR}(i)}(s) \cdot \prod_{i=1}^{n} K_{\mathrm{iBR}(i)}(s). \quad (11)$$

Our example focuses on a four section-based comb filter that generates two sBR and two iBR responses. The total number of sections is $n = 2$ of each type of filter (four sections in total). The essential block connection is shown in Fig. 3(a). Further explanation of the design is provided in Fig. 3(b) where parameters of sections are defined.

Table III summarizes the design specifications of the used sections in the resulting comb filter. The design equations valid for sBR(i) sections are as follows: $g_{mb(i)} = C_{(i)} \cdot (2\pi BW_s)$, $g_{ma(i)} = (1-|K_{\min}(f = f_{C(i)})|) \cdot g_{mb(i)}$, and $R_{(i)} = g_{mb(i)}/(2\pi f_{C(i)}C_{(i)})^2$. The iBR($i$) sections have only slightly different formulas: $g_{mb(i)} = C_{(i)} \cdot (2\pi BW_i)/|K_{\max}(f = f_{C(i)})|$ and $g_{ma(i)} = (|K_{\max}(f = f_{C(i)})|-1) \cdot g_{mb(i)}$. The formula for $R_{(i)}$ is identical for both cases.

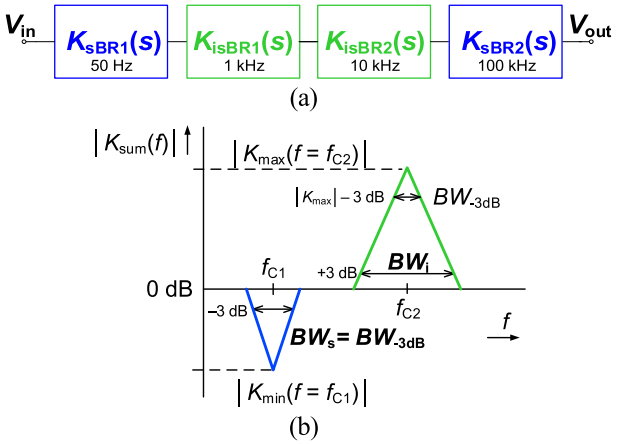

Fig. 3. Comb filter (a) block structure and (b) parameters explanation.

TABLE III
Ideal Specifications of Comb Filter Sections

section (i)	1	1	2	2
type	sBR_1	iBR_1	iBR_2	sBR_2
$f_{C(i)}$ [kHz]	0.05	1.00	10.00	100.00
$BW_{s/i(i)}$ [kHz]	0.01	1.00	7.00	10.00
$\lvert K_{\max/\min}(f=f_{C(i)})\rvert$ [dB]	–20	+26	+17	–30
$C_{a(i)} = C_{b(i)} = C_{(i)}$ [nF]	1 000	100	10	10
$R_{(i)}$ [Ω] (E24 series)	636 (620)	80 (82)	160 (160)	16 (16)
$g_{ma(i)}$ [μS]	57	596	377	610
$g_{mb(i)}$ [μS]	63	31	63	628

IV. Experimental Verification

The simulations were conducted using PSPICE, while all experiments were performed by Keysight DSO-X 3024T oscilloscope, which features an in-built wave-generator and Bode plot (frequency response analysis) option.

A. Comparison of Design Targets, Simulation, and Experiment

Due to the characteristics of the LT1228 [31], the applied voltage amplitude levels used in tests were set to the tens of millivolts. The supply voltage was set at ±5 V. The bias currents [31] for electronic adjustment can be calculated as $I_{\mathrm{seta/b(i)}} = g_{ma/b(i)}/10$. The R_{stab} resistor in Fig. 2 improves the stability of the solution without affecting the functionality when current input terminal (–) is loaded by the parasitic grounded capacity of the metal wires of the printed circuit board (although it can be omitted when not necessary). This relates to the high transimpedance gain of the CFOA part. It has not impact on declared operational band. The interconnection of $IC_{b(i)}$ (from the CFOA output to the OTA negative input) establishes a global negative feedback. However, it does not produce a pure voltage follower due to high-impedance node between the OTA and CFOA being connected to $C_{a(i)}$, as well as the CFOA negative input being connected to the feedback loop through $C_{b(i)}$ and $R_{(i)}$. Table IV presents comparison of targeted and experimentally obtained results. The measured magnitude transfer responses are shown in Fig. 4 for all tested sections independently.

TABLE IV
SPECIFICATIONS OF COMB FILTER SECTIONS (IDEAL EXPECTATIONS AND DESIGN TARGETS)

	ideal (design target)	measured	deviation from ideal
sBR$_1$			
f_{C1} [kHz]	0.05 (0.048↔0.052)	0.051	0.001 (2%)
BW_s [kHz]	0.01 (0.008↔0.012)	0.011	0.001 (10%)
$\lvert K_{min}(f=f_{C1})\rvert$ [dB]	–20 (–18↔–21)	–18.8	1.2 (–6%)
iBR$_1$			
f_{C1} [kHz]	1.0 (0.9↔1.1)	0.96	0.04 (–4%)
BW_i [kHz]	1.0 (0.8↔1.2)	1.20	0.20 (20%)
BW_{-3dB} [kHz]	0.05 (0.04↔0.06)	0.053	0.003 (6%)
$\lvert K_{max}(f=f_{C1})\rvert$ [dB]	+26 (+24↔+27)	+25.5	0.5 (–2%)
iBR$_2$			
f_{C2} [kHz]	10 (9↔11)	10.1	0.1 (1%)
BW_i [kHz]	7 (6↔8)	7.8	0.8 (11%)
BW_{-3dB} [kHz]	1 (0.8↔1.2)	1.17	0.17 (17%)
$\lvert K_{max}(f=f_{C2})\rvert$ [dB]	+17 (+15↔+18)	+16.2	0.8 (–5%)
sBR$_2$			
f_{C2} [kHz]	100 (98↔102)	99.5	0.5 (–0.5%)
BW_s [kHz]	10 (8↔12)	11.9	1.9 (19%)
$\lvert K_{min}(f=f_{C2})\rvert$ [dB]	–30 (–28↔–31)	–29.4	0.6 (–2%)

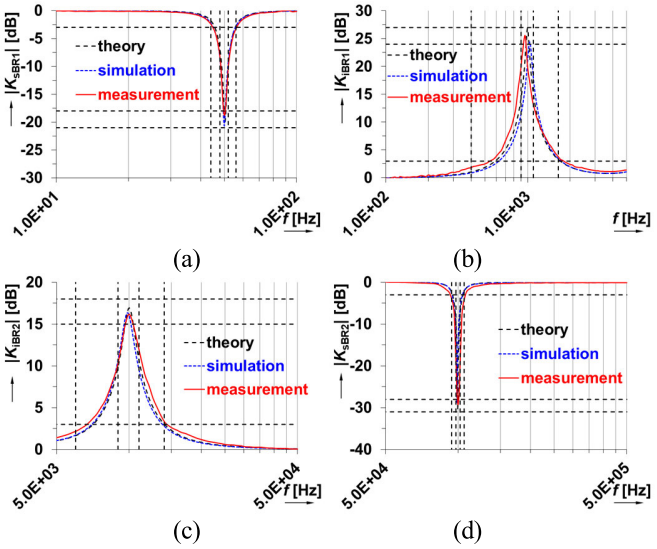

Fig. 4. Detail on partial magnitude responses of the comb filter. (a) sBR$_1$, (b) iBR$_1$, (c) iBR$_2$, and (d) sBR$_2$.

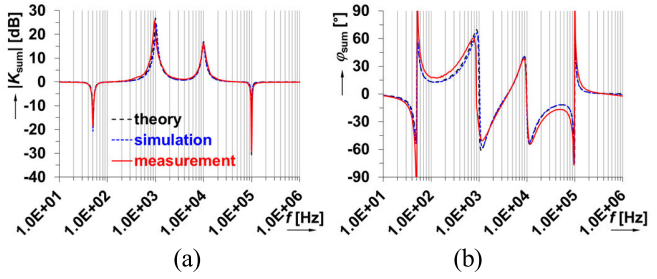

Fig. 5. Full frequency response of the comb filter. (a) Magnitude plot and (b) phase plot.

Dashed lines indicate the allowed tolerances of the design targets. Fig. 5 illustrates the complete frequency response of the comb filter when all four blocks are connected as a cascade.

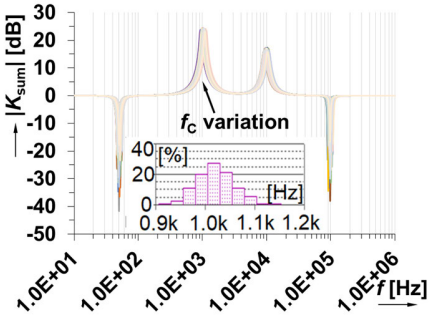

Fig. 6. Magnitude frequency responses of the comb filter in tolerance analysis (1000 runs).

TABLE V
SIMULATED STATISTICAL VARIATION OF PASSIVE ELEMENTS (RESULTS OF MONTE CARLO SWEEP)

section (i)	1	1	2	2
type	sBR$_1$	iBR$_1$	iBR$_2$	sBR$_2$
$f_{C(i)\_min}$ [kHz]	0.046	0.90	8.90	89.11
$f_{C(i)\_max}$ [kHz]	0.056	1.15	11.12	110.01
$f_{C(i)\_mean}$ [kHz]	0.050	1.02	9.86	98.95
sigma [kHz]	0.002	0.037	0.345	3.648
$BW_{s/i(i)\_min}$ [kHz]	0.0095	0.86	6.02	8.82
$BW_{s/i(i)\_max}$ [kHz]	0.012	1.17	7.69	11.80
$BW_{s/i(i)\_mean}$ [kHz]	0.011	1.00	6.77	10.16
sigma [kHz]	0.0004	0.05	0.29	0.47
$\lvert K_{max/min}(f=f_{C(i)})\rvert_{\_min}$ [dB]	–44.0	+22.0	+14.7	–43.4
$\lvert K_{max/min}(f=f_{C(i)})\rvert_{\_max}$ [dB]	–11.5	+24.8	+17.6	–9.8
$\lvert K_{max/min}(f=f_{C(i)})\rvert_{\_mean}$ [dB]	–19.5	+23.5	+16.3	–18.3
sigma [dB]	4.4	0.5	0.5	5.0
tol. C = 5%, tol. R = 1%				

B. Analysis of Statistical Variation of Circuit Elements

The statistical variation of passive components, assuming a 1% tolerance for resistors and a 5% tolerance for capacitors, is shown in Fig. 6 (Monte Carlo sweep for 1000 runs). The results of the analyses (histograms) are summarized in Table V. The statistical dispersion of component values is most pronounced at the center frequencies corresponding to the points of maximum gain or attenuation (s/iBR peaks). This occurs due to the form of (1), where the mismatch of capacitors (which have the largest tolerances in the design) directly affects the gain/attenuation of the section. This impact is the most significant for attenuation. Fortunately, these features can be adjusted by $g_{ma(i)}$ and can be easily compensated for during the testing phase or during full operation of the device. The Gaussian variation (5%) of both $I_{seta/b(i)}$ for controlling $g_{ma/b(i)}$ has an effect comparable to the variation of passive elements shown in Table V. However, these effects can be easily compensated through electronic control of both parameters.

C. Linearity and THD

The total harmonic distortion (THD) of the comb filter ranges from 0.1% to 0.2% for an input level of 50 mV$_{p-p}$ and reaches 0.8% for 100 mV$_{p-p}$ at a test frequency of 200 Hz in the passband area (outside of f_{Ci}). At the highest peak of the comb filter (f_C = 1 kHz), the distortion reaches 1% for input levels below 25 mV$_{p-p}$. These values are typical

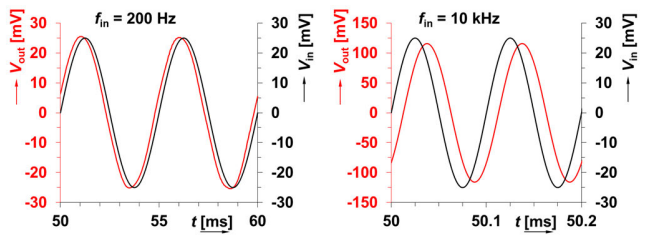

Fig. 7. Examples of time-domain responses of the comb filter in (a) passband 200 Hz and (b) maximal gain at 10 kHz.

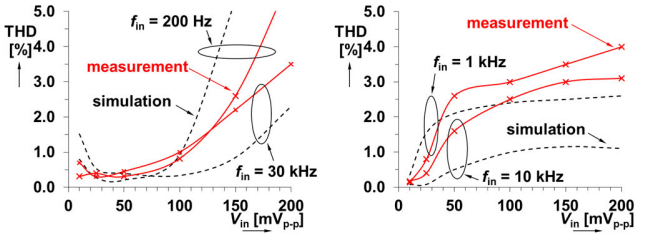

Fig. 8. Dependence of THD on input level for selected testing frequencies (a) passbands and (b) gain maximums.

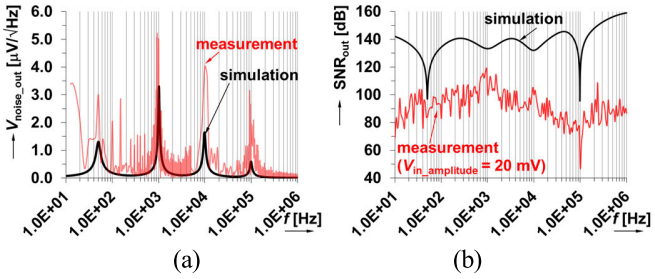

Fig. 9. Simulation and measurement of the noise performance (a) output referred noise voltage in the observed operational bandwidth and (b) SNR in the operational bandwidth.

when linearizing resistor dividers, as recommended in [31], are not used. Including these dividers improves the linearity of the OTA section of LT1228, allowing operation at input levels up to several volts with THD below 1%. However, this comes at the cost of reducing the available OTA g_m range and increasing noise issues and overall complexity. Examples of time-domain responses are shown in Fig. 7 for input frequencies of 200 Hz and 10 kHz. The dependence of THD on input level across various frequencies within the operational band (passband areas and selected f_C frequencies) highlights the nonlinear characteristics of the filter, as illustrated in Fig. 8. The simulated responses differ from measured responses at the frequencies of gain maximums because real features that do not perfectly match the simulated case. These discrepancies arise from slight inaccuracies in the settings—such as slightly different f_C of the highly selective section—and the combined impact of nonlinearity in the transfer response at varying signal levels and frequency-dependent large signal behavior.

D. Noise Performance

The results of noise analysis are shown in Fig. 9. The trace reflects the shape of the filter's response, with the output signal-to-noise ratio (SNR) reaching around 80 dB in wide

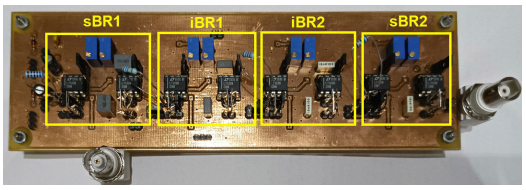

Fig. 10. Developed prototype of comb filter.

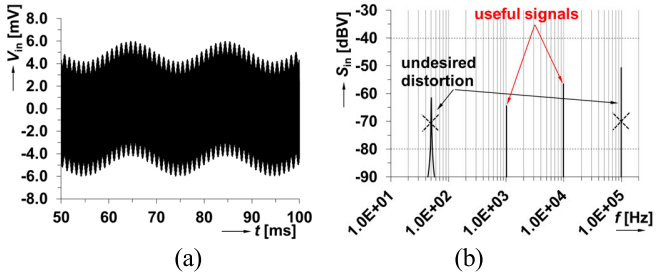

Fig. 11. Complex input signal of four harmonic components (two are undesired) (a) time domain and (b) FFT spectrum.

frequency range for a passband signal amplitude of 20 mV (linearly processed, see Fig. 8) in real experiments. The selective peaks in the response are attributed to the attenuation subbands of the filter, with the most critical points being the f_C frequencies of attenuation. It is important to note that the simulation-based results, which differ significantly from the measurement-based results, are based on a circuit model that assumes ideal interconnections (without parasitic effects, printed circuit board interconnections, and so on). The difference of simulated and measured trace shape exists due to limited accuracy of measuring device. The measured results, depicted in red, were obtained using an Agilent 4395 A vector/network/spectrum/impedance analyzer. The experimental prototype is shown in Fig. 10.

V. Application Example—Equalization of Selective Signals and Distortions

Fig. 11 captures a typical scenario in many communication and industrial systems, and instruments. The situation described next is common for systems operating in kilo-Hertz audio bands, such as signal processing in sensing applications [29], [30].

The signal spectrum consists of several narrowband signals or spectral components obtained by arbitrary signal generators, some essential for system operation and others unwanted, causing distortion. Each of these signals requires appropriate processing, either attenuation or amplification. For example, the desired signals crucial for the system are spectral components at frequencies of 1 and 10 kHz, with levels of −66 and −57 dBV, respectively (intentionally unbalanced). These frequencies may represent so-called signal tones used for duplex digital communication systems [33]. Further processing requires both signaling frequencies to be evenly amplified to −40 dBV (10 mV in amplitude). Distorting signals at 50 Hz and 100 kHz must be attenuated according to the system's tolerance mask, keeping their levels below −80 dBV. The distortion at 100 kHz has a more significant impact, so a 30 dB attenuation is needed in this subband. The advantages of the selective response adjustments

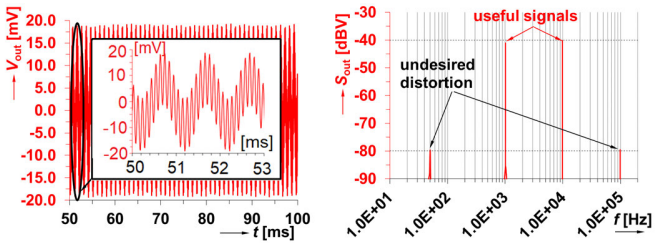

Fig. 12. Output response of the comb filter (a) time domain and (b) FFT spectrum.

(attenuation and amplification) in subbands of the comb filter prove highly beneficial in this application. The response of the comb filter, as shown in Fig. 5 and discussed earlier, enables precise tuning. The resulting output response is shown in Fig. 12. In comparison, standard second-order bandpass and band-reject filters (which may require increased complexity for adjustability) are less effective in this application due to the monotonic rise and fall of the magnitude response between subbands. The special comb filter, however, creates flat areas between selective responses, offering superior performance.

The advantages of presented solution and application (Figs. 11 and 12) are beneficial for instrumentation and sensing field especially in analog preprocessing of very complex and distorted signals [34] or signals from resonant sensors (having resonant-peaking character of frequency response) [29], [35], as (pre or post) compensation of imbalances [29], [35], [36].

VI. Conclusion

The proposed solution of the comb filter holds importance in the field of equalization and compensation of frequency imbalances in modern sensing readouts. The propagation of signals or sensed quantities through various materials often results in selective absorptions and distortions. We introduced a special filtering section for the generation of band-reject and inverting band-reject responses. The design of the section is straightforward, and the degree of freedom afforded by the specific solution allows for the selection of identical values of capacitors ($C_{a(i)} = C_{b(i)}$) from fabrication series. Four of these sections were connected in cascade with center frequencies of 50 Hz, 1 kHz, 10 kHz, and 100 kHz (see details in Tables III and IV). The center frequency and attenuation/amplification indicate good accuracy (with errors in units of percent) regarding theoretical targets. The most significant deviations from ideal values occur in bandwidth (approximately 10%–20%), but they still fulfill design targets. The measured response of the complete comb filter indicates minimal impact of the real features of the used devices in the observed range up to 1 MHz. Future efforts will be focused on modifying the solution to provide full independence in setting and adjusting gain/attenuation, bandwidth, and center frequency of the sections.

VII. Acknowledgment

This work was supported by the Internal Grant of Brno University of Technology (BUT) under Project FEKT-S-23-8191. This project has received funding from the Research Council of Lithuania (LMTLT), Agreement No. S-AUEI-23-1 (22-12-2023). This work was supported by the Institutional Support of the Ministry of Defence of the Czech Republic.

References

[1] L. Morán et al., *Power Electronics Handbook: Active Filters*. Amsterdam, The Netherlands: Elsevier, Jan. 2024, pp. 1301–1341, doi: 10.1016/b978-0-323-99216-9.00035-4.

[2] V. H. Nascimento and T. M. M. Silva, *Power Electronics Handbook: Adaptive Filters*. Amsterdam, The Netherlands: Elsevier, Jan. 2024, pp. 717–868, doi: 10.1016/b978-0-32-391772-8.00018-1.

[3] C.-T. Tsai, H.-L. Chan, C.-C. Tseng, and C.-P. Wu, "Harmonic interference elimination by an active comb filter [ECG application]," in *Proc. 16th Annu. Int. Conf. IEEE Eng. Med. Biol. Soc.*, Baltimore, MD, USA, Nov. 1994, pp. 964–965, doi: 10.1109/IEMBS.1994.415235.

[4] R. K. Ranjan, S. P. Yalla, S. Sorya, and S. K. Paul, "Active comb filter using operational transconductance amplifier," *Act. Passive Electron. Compon.*, vol. 2014, pp. 1–6, Jan. 2014, doi: 10.1155/2014/587932.

[5] C. K. Choubey, A. Sahani, and S. K. Paul, "Ultra-low power comb filter," in *Proc. IEEE Int. Conf. (ICAECCT)*, Pune, India, Jun. 2016, pp. 164–166, doi: 10.1109/ICAECCT.2016.7942575.

[6] R. K. Ranjan, C. K. Choubey, B. C. Nagar, and S. K. Paul, "Comb filter for elimination of unwanted power line interference in biomedical signal," *J. Circuits, Syst. Comput.*, vol. 25, no. 6, Mar. 2016, Art. no. 1650052, doi: 10.1142/s0218126616500523.

[7] S. K. Paul, C. K. Choubey, and G. Tiwari, "Low power analog comb filter for biomedical applications," *Anal. Integr. Circuits Signal Process.*, vol. 97, no. 2, pp. 371–386, Sep. 2018, doi: 10.1007/s10470-018-1329-8.

[8] C. K. Choubey, A. Kanungo, A. Srivastava, and A. Gupta, "PLI cancellation from biomedical signals using VDTA-based notch/comb filter," in *Proc. 3rd Asian Conf. Innov. Technol. (ASIANCON)*, Ravet IN, India, Aug. 2023, pp. 1–6, doi: 10.1109/asiancon58793.2023.10270160.

[9] C. K. Choubey, S. Kumar, and S. K. Pippal, "Design method for VDCC-based analog comb filter for power line interference cancellation," *MethodsX*, vol. 12, Jun. 2024, Art. no. 102619, doi: 10.1016/j.mex.2024.102619.

[10] S. S. Gupta, D. R. Bhaskar, R. Senani, and A. K. Singh, "Inverse active filters employing CFOAs," *Electr. Eng.*, vol. 91, no. 1, pp. 23–26, May 2009, doi: 10.1007/s00202-009-0112-3.

[11] H.-Y. Wang, S.-H. Chang, T.-Y. Yang, and P.-Y. Tsai, "A novel multifunction CFOA-based inverse filter," *Circuits Syst.*, vol. 2, no. 1, pp. 14–17, Jan. 2011, doi: 10.4236/cs.2011.21003.

[12] A. Raj, R. Bhagat, P. Kumar, and D. R. Bhaskar, "Grounded-capacitor analog inverse active filters using CMOS OTAs," in *Proc. 8th Int. Conf. Signal Process. Integr. Netw. (SPIN)*, Noida, India, Aug. 2021, pp. 778–783, doi: 10.1109/SPIN52536.2021.9566076.

[13] P. Kumar, N. Pandey, and S. K. Paul, "Realization of resistorless and electronically tunable inverse filters using VDTA," *J. Circuits, Syst. Comput.*, vol. 28, no. 9, Aug. 2019, Art. no. 1950143, doi: 10.1142/s0218126619501433.

[14] R. Bhagat, D. R. Bhaskar, and P. Kumar, "Multifunction filter/inverse filter configuration employing CMOS CDBAs," *Int. J. Recent Technol. Eng. (IJRTE)*, vol. 8, no. 4, pp. 8844–8853, Nov. 2019, doi: 10.35940/ijrte.d9476.118419.

[15] S. S. Borah, A. Singh, and M. Ghosh, "CMOS CDBA based 6th order inverse filter realization for low-power applications," in *Proc. IEEE REGION 10 Conf. (TENCON)*, Osaka, Japan, Nov. 2020, pp. 11–15, doi: 10.1109/TENCON50793.2020.9293817.

[16] R. Pandey, N. Pandey, T. Negi, and V. Garg, "CDBA based universal inverse filter," *ISRN Electron.*, vol. 2013, pp. 1–6, Mar. 2013, doi: 10.1155/2013/181869.

[17] T. K. Paul, S. Roy, and R. R. Pal, "Realization of inverse active filters using single current differencing buffered amplifier," *J. Sci. Res.*, vol. 13, no. 1, pp. 85–99, Jan. 2021, doi: 10.3329/jsr.v13i1.47766.

[18] A. K. Singh, A. Gupta, and R. Senani, "OTRA-based multi-function inverse filter configuration," *Adv. Electr. Electron. Eng.*, vol. 15, no. 5, pp. 846–856, Jan. 2018. [Online]. Available: https://www.researchgate.net/publication/322530870_OTRA-Based_Multi-Function_Inverse_Filter_Configuration

[19] S. M. Al-Shahrani and M. A. Al-Absi, "Efficient inverse filters based on second-generation voltage conveyor (VCII)," *Arabian J. Sci. Eng.*, vol. 47, no. 3, pp. 2685–2690, Jun. 2021, doi: 10.1007/s13369-021-05775-5.

[20] M. A. Al-Absi, "Realization of inverse filters using second generation voltage conveyor (VCII)," *Anal. Integr. Circuits Signal Process.*, vol. 109, no. 1, pp. 29–32, Oct. 2021, doi: 10.1007/s10470-021-01874-3.

[21] R. Senani, D. R. Bhaskar, and A. Raj, "Inverse analog filters: History, progress and unresolved issues," *Electronics*, vol. 11, no. 6, p. 841, Mar. 2022, doi: 10.3390/electronics11060841.
[22] T. Tsukutani, Y. Sumi, and N. Yabuki, "Electronically tunable inverse active filters employing OTAs and grounded capacitors," *Int. J. Electron. Lett.*, vol. 4, no. 2, pp. 166–176, Dec. 2014, doi: 10.1080/21681724.2014.984636.
[23] P. Kumar, N. Pandey, and S. K. Paul, "Electronically tunable VDTA-based multi-function inverse filter," *Iranian J. Sci. Technol., Trans. Electr. Eng.*, vol. 45, no. 1, pp. 247–257, Jun. 2020, doi: 10.1007/s40998-020-00355-z.
[24] C. Psychalinos, S. Minaei, and A. Yesil, "First-order inverse filters: Implementations using a single voltage conveyor and potential applications," *Int. J. Circuit Theory Appl.*, vol. 50, no. 10, pp. 3704–3714, Jun. 2022, doi: 10.1002/cta.3346.
[25] J. Nako, C. Psychalinos, and S. Minaei, "Single-input multiple-output inverse filters designs with cascade capability," *AEU-Int. J. Electron. Commun.*, vol. 175, Feb. 2024, Art. no. 155061, doi: 10.1016/j.aeue.2023.155061.
[26] J. Nako and C. Psychalinos, "Formant filters designs with adjustable characteristics," in *Proc. Panhellenic Conf. Electron. Telecommun. (PACET)*, Thessaloniki, Greece, 2024, pp. 1–4, doi: 10.1109/PACET60398.2024.10510194.
[27] J. Nako, G. Tsirimokou, and C. Psychalinos, "Adjustable resonator and anti-resonator designs for speech signal processing," *AEU-Int. J. Electron. Commun.*, vol. 183, Aug. 2024, Art. no. 155382, doi: 10.1016/j.aeue.2024.155382.
[28] K. Kim and S.-C. Liu, "Continuous-time analog filters for audio edge intelligence: Review on circuit designs [feature]," *IEEE Circuits Syst. Mag.*, vol. 23, no. 2, pp. 29–48, 2nd Quart., 2023, doi: 10.1109/MCAS.2023.3267893.
[29] R. Sotner et al., "Special transfer section for selective rejecting and amplification of bands in equalization," *IEEE Trans. Circuits Syst. I, Reg. Papers*, vol. 71, no. 9, pp. 3986–3998, Sep. 2024, doi: 10.1109/TCSI.2024.3408691.
[30] S. Yadav, P. A. D. Legaspi, M. S. O. Alink, A. B. J. Kokkeler, and B. Nauta, "Hardware implementations for voice activity detection: Trends, challenges and outlook," *IEEE Trans. Circuits Syst. I, Reg. Papers*, vol. 70, no. 3, pp. 1083–1096, Mar. 2023, doi: 10.1109/TCSI.2022.3225717.
[31] *Linear Technology, Analog Devices, LT1228 100 MHz Current Feedback Amplifier With DC Gain Control, Datasheet*. Accessed: 29, Feb. 2024. [Online]. Available: https://www.analog.com/media/en/technical-documentation/data-sheets/1228fd.pdf
[32] T. Yucehan and E. Yuce, "A new grounded capacitance multiplier using a single ICFOA and a grounded capacitor," *IEEE Trans. Circuits Syst. II, Exp. Briefs*, vol. 69, no. 3, pp. 729–733, Mar. 2022, doi: 10.1109/TCSII.2021.3102118.
[33] A. Imran, Y. Sun, D. Niyato, and L. Zhang, *Wireless Semantic Communications: Concepts, Principles and Challenges*, 1st ed., Hoboken, NJ, USA: Wiley, 2025.
[34] N. Zheng and Y. Li, "Recognition of muscular activity in complex noise-contaminated myoelectric signals: An adaptive two-step approach," *IEEE Trans. Instrum. Meas.*, vol. 73, pp. 1–13, 2024, doi: 10.1109/TIM.2024.3351258.
[35] H. A. Brausen and J. C. Sit, "A bridge-balancing circuit for balanced measurement of resonant sensors," *IEEE Trans. Instrum. Meas.*, vol. 69, no. 7, pp. 5002–5009, Jul. 2020, doi: 10.1109/TIM.2019.2954146.
[36] S. F. Syeda, M. Crescentini, M. Marchesi, P. A. Traverso, and A. Romani, "A wideband and low-noise CMOS-integrated X-Hall current sensor operating in current mode," *IEEE Trans. Instrum. Meas.*, vol. 72, pp. 1–11, 2023, doi: 10.1109/TIM.2023.3284055.

Roman Sotner (Member, IEEE) was born in Znojmo, Czech Republic, in 1983. He received the M.Sc. and Ph.D. degrees in electrical engineering from Brno University of Technology (BUT), Brno, Czech Republic, in 2012 and 2008, respectively.

He is currently an Associate Professor with the Department of Radio Electronics, Faculty of Electrical Engineering and Communication, BUT. His research interests include discrete as well as integrated analog circuits (active filters, oscillators, audio, and so on), circuits in the current mode, circuits with direct electronic controlling possibilities, especially analog signal processing in sensing applications, and computer simulation.

Dmitrii Semenov is currently pursuing the master's degree with the Department of Radio Electronics, Faculty of Electrical Engineering and Communication, Brno University of Technology (BUT), Brno, Czech Republic.

He is an Analog Design Intern at Semiconductor Supplier "Onsemi." His research interests include integrated analog circuits (active filters, operational amplifiers, references, and so on), analog signal processing, circuit design based on operational transconductance amplifiers, and global optimization methods.

Darius Andriukaitis (Member, IEEE) received the M.Sc. and Ph.D. degrees in electronics engineering from Kaunas University of Technology, Kaunas, Lithuania, in 2005 and 2009, respectively.

He works at the Department of Electronics Engineering, Faculty of Electrical and Electronics Engineering, Kaunas University of Technology. He is also the Vice Dean for Research at the Faculty of Electrical and Electronics Engineering. His research interests include finding solutions for the issues related to interactive electronic systems, integrated information systems, or WSN.

Marek Svoboda was born in Havlíčkův Brod, Czech Republic, in 1999. He received the bachelor's degree in Electronics and Communication Technologies from the Faculty of Electrical Engineering and Communication, Brno University of Technology (BUT), Brno, Czech Republic, in 2021, and the M.Sc. degree in the same field, in 2023, where he is currently pursuing the Ph.D. degree.

His research interests are directed toward the sensing and signal processing systems and design of analog integrated circuits.

Ladislav Polak (Member, IEEE) was born in Štúrovo, Slovakia, in 1984. He received the M.Sc. and Ph.D. degrees in electronics and communication from Brno University of Technology (BUT), Brno, Czech Republic, in 2009 and 2013, respectively.

He is currently an Associate Professor with the Department of Radio Electronics (DREL), BUT. His research interests include wireless communication systems, RF measurements, and computer-aided analysis.